Experimental Thermal and Fluid Science 151 (2024) 111097

Contents lists available at ScienceDirect

Experimental Thermal and Fluid Science

journal homepage: www.elsevier.com/locate/etfs

Influence of a surfactant on bubble bursting

E.J. Vega *, J.M. Montanero

Depto. de Ingeniería Mecánica, Energética y de los Materiales and Instituto de Computación Científica Avanzada (ICCAEx), Universidad de Extremadura, E-06006 Badajoz, Spain

ARTICLE INFO

Keywords:
Bubble bursting
Surfactant
Droplet
Aerosols

ABSTRACT

We study the bursting of a bubble covered with a surfactant experimentally. We conclude that the bubble bursting takes longer than that of a surfactant-free bubble with the same equilibrium surface tension due to the interfacial elasticity. A tiny bubble is formed at the cavity bottom right before the free surface reversal due to the Marangoni stress. This stress also drives the liquid flow that makes the jet escape from the end-pinching mechanism for a certain surfactant concentration interval. A diminutive liquid droplet manages to escape from the jet for a sufficiently large surfactant concentration. This droplet is much smaller than its surfactant-free counterpart but moves at a similar speed. The surfactant molecules are convected toward the jet tip so that the monolayer covering the first-emitted droplet is practically saturated.

1. Introduction

Fine and ultra-fine atmospheric aerosols produced from the ocean surface are fundamental regulators of atmospheric physics. They determine the nucleation of supersaturated water vapor in the atmosphere, the formation of clouds that regulate the albedo effect of the planet, and the generation of droplets of sufficient size to cause rain or ice crystals of very diverse structure and sizes [1].

The fine ocean spray generated at the water–air turbulent interface is the major source of fine aerosols. Different phenomena produce the fragmentation of water into micrometer and sub-micrometer droplets. Among them, the bursting of small bubbles on the liquid surface is the most ubiquitous and universally widespread [2]. This phenomenon has only recently begun to be investigated in depth both theoretically [3–8] and experimentally [2,5,9,10].

The bubble bursting has been described as follows [8]. Two capillary wavefronts are triggered at the initial stage of the bubble bursting: one propagating away from the cavity and the other moving over the bubble surface toward its bottom. We here focus on the latter, which is responsible for jet formation. In the parameter region of interest, the short-wavelength domain of the spectrum (the wavelets) contains a significant portion of the wavefront energy. These wavelets arrive first at the bottom but do not produce any significant effect. The jet is formed by the long-wavelength toroidal capillary wave containing most of the interfacial energy. This wave becomes steeper when converging at the bubble bottom, causing a collapsing radial flow that reverses the bubble surface. Under certain conditions, the free surface reversal is preceded by its pinching, which produces a tiny bubble trapped below the jet [11]. After the free surface reversal, the excess of the liquid kinetic energy goes in two opposite directions along the symmetry axis, producing two vortices and a liquid jet in the downward and upward directions, respectively. The jet may break up while moving upwards due to the end-pinching mechanism. This process results in the so-called jet droplets.

Bubble bursting in the presence of compound [12] and oil-coated interfaces [13] has been examined experimentally. Studies of the effect of surfactants on bubble bursting are still very scarce despite the ubiquity of these contaminants in natural and technological processes. Numerical simulations [11] have shown that surfactant molecules are swept toward the bottom during the cavity collapse, resulting in varying surfactant concentrations at the interface. The resulting Marangoni stresses affect the cavity collapse and the jet emission and breakup. The monolayer dilatational viscosity can slow and even prevent the formation of a liquid jet [14].

Experimental results have recently been obtained with Sodium Dodecyl Sulfate (SDS) [15]. In general, fewer droplets were produced than for the corresponding clean interface. In some cases, the surfactant monolayer suppressed the emission of jet droplets. Despite these novel results, the bursting of surfactant-covered bubbles needs to be revisited.

In the present work, dimensional analysis and comparison with the bursting of the surfactant-free bubbles will allow us to determine the roles played by the local reduction of surface tension (the local soluto-capillarity effect) and the Marangoni stress (interfacial elasticity) during the cavity collapse, the jet formation, and the ejection of the droplets.

* Corresponding author.
E-mail address: ejvega@unex.es (E.J. Vega).

https://doi.org/10.1016/j.expthermflusci.2023.111097
Received 15 June 2023; Received in revised form 7 September 2023; Accepted 5 November 2023
Available online 8 November 2023

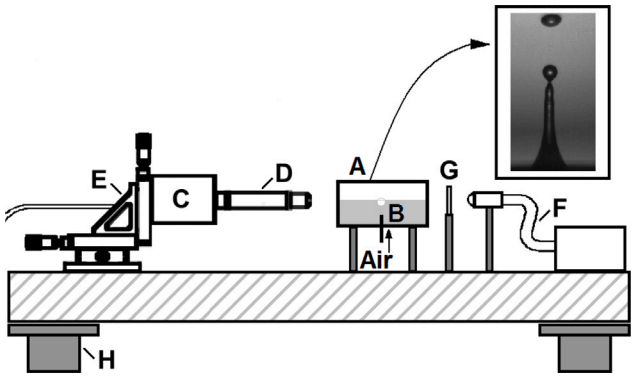

Fig. 1. Experimental setup: tank filled with the working liquid (A), needle (B), camera (C), optical lenses (D), triaxial translation stage (E), optical fiber (F), and pneumatic anti-vibration isolation system (H).

2. Experimental method

We used a parallelepipedal glass tank 10 cm in length and width, and 7 cm in depth (Fig. 1). The tank was filled with the working liquid to conduct the experiments. For moderate and large surfactant concentrations, a large (in terms of the bubble size) capillary meniscus formed on the tank walls, hindering the bubble's visualization. To reduce the effect of the meniscus on the images, we needed to use optical lenses with a lower depth of field and tilt the camera 2° with respect to the liquid free surface. Unfortunately, this inevitably limited the sharpness of the images of the cavity wave collapse. Nevertheless, the images were sufficiently sharp to describe the surfactant effect on the bubble bursting.

We used two needles 0.190 and 0.146 mm in outer diameter and 0.1 mm in inner diameter to change the bubble size. The needles were positioned in an orifice in the center of the tank bottom. We used a syringe pump (KDS Legato 210) to inject air through the needle quasi-statically. The bubble detached from the needle and rose across the tank until reaching the free surface. Then, it remained there for several seconds and burst. As shown below, this time interval was sufficiently long for the monolayer to reach the equilibrium.

The bubble bursting was recorded with a high-speed video camera (Photron, Fastcam Mini UX50) at 8000 fps with an exposure time of 12.5 μs. The images were comprised of 296 × 1280 pixels. The camera was equipped with a set of optical lenses consisted of an objective HR 2/300 F2.8/50 mm (Goyo Optical Inc.), extending rings 40 mm in length, and a zoom 2×. The magnification obtained was approximately 6.4 μm/pixel.

The camera could be displaced horizontally and vertically using a triaxial translation stage to focus the bubble. The fluid configuration was illuminated from the backside by cool white light provided by an optical fiber. All these elements were mounted on an optical table with a pneumatic anti-vibration isolation system to damp the vibrations coming from the building.

We dissolved SDS (PanReac AppliChem, SDS for molecular biology) in distilled water (Guinama, demineralized water) to study the effects of a surfactant monolayer on the bubble bursting. The adsorption and desorption characteristic times of SDS are of the order of 0.1 s [16,17], much smaller than the bubble residence time before bursting. Therefore, one can safely assume that the monolayer becomes at equilibrium with the surfactant sublayer before the bubble bursts. The bulk and surface diffusivities are 1×10^{-10} m^2/s and 8×10^{-10} m^2/s, respectively [17]. The surface shear and dilatational viscosities take very small values [18].

Fig. 2 shows the dependence of the surface tension σ and surfactant surface density $\hat{\Gamma}$ on the volumetric surfactant concentration c. The figure also shows σ as a function of $\hat{\Gamma}$, which allows one to assess the intensity of the Marangoni stress. The critical micellar concentration is $c_{\rm cmc} \simeq 8$ mM/kg, and the maximum surface density is $\hat{\Gamma}_\infty \simeq 3.2$ μmol/m^2. The liquid density and viscosity are approximately the same as those of distilled water ($\rho = 998$ kg/m^3 and $\mu = 1.0$ mPa·s). Table 1 shows the surface tension and bubble radius of the experiments analyzed in this work.

SDS exhibits a relatively singular behavior for a surface density around the saturation value $\hat{\Gamma}_\infty$. The surface density reaches an approximately constant value while the surface tension experiences significant variations (Fig. 2c). This implies that variations of c can significantly affect the bubble bursting even if they cause very small variations of the initial (equilibrium) value $\hat{\Gamma}_{\rm eq}$ around $\hat{\Gamma}_\infty$. For this reason, we will distinguish between quasi-saturated and saturated monolayers.

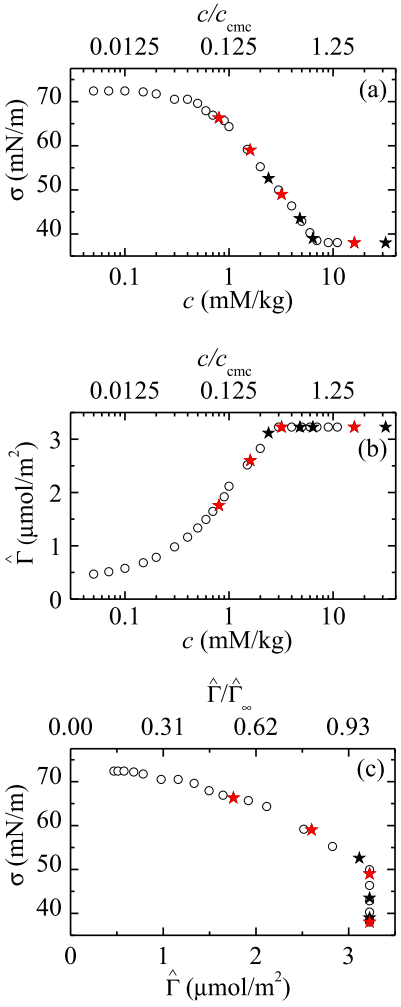

Fig. 2. Experimental values of $\sigma(c)$, $\hat{\Gamma}(c)$, and $\sigma(\hat{\Gamma})$ [19]. The stars indicate the cases studied in this work. The red symbols are those compared with experiments without surfactant.

Table 1
Surfactant concentration c, surface tension σ, and bubble radius R for the experiments with surfactant analyzed in this work [19].

c (mM/kg)	σ (mN/m)	R (mm)
0.8	66.3	0.979
1.6	59.0	0.941
2.4	52.6	0.929
3.2	49.0	0.889
4.8	43.5	0.834
6.4	39.0	0.789
16.0	38.0	0.713
32.0	38.0	0.714

Table 2
Density ρ, viscosity μ, surface tension σ, and bubble radius R for the mixtures of glycerol and water. The density and viscosity values were taken from the literature [20], while the surface tension was measured with the Theoretical Interface Fitting Analysis (TIFA) method [21].

Mixture WXGY	ρ (kg/m^3)	μ (mPa s)	σ (mN/m)	R (mm)
W95G5	1010	1.147	66 ± 1	1.000
W91G9	1020	1.277	65 ± 1	0.990
W85G15	1036	1.547	60 ± 1	0.876

We also conducted experiments without surfactants to determine the effects of the surfactant monolayer on the bubble bursting, as explained in Section 3. Mixtures of glycerol (PanReac AppliChem, glycerol 99% for synthesis) and distilled water were used for this purpose. The glycerol concentration was selected to ensure that the relevant dimensionless numbers took approximately the same values with and without surfactant (see Section 3). We will refer to these solutions as WXGY, where "X" and "Y" indicate the relative concentrations in weight of water and glycerol, respectively. The properties of these mixtures are shown in Table 2, besides the bubble radius R obtained and studied in each case.

It must be noted that all the working solutions were used during the first 24 h after their production (normally, right after their production) to reduce the effect of surfactant aging and ambient impurities. This considerably increases the reproducibility of the results.

We repeated each experiment five times and verified that they were highly reproducible. For instance, the diameter of the first-ejected droplet varied by less than 10% when the experiment was repeated. The error bars shown in the figures of Section 4 correspond to the standard deviations.

3. Dimensional analysis

In an experiment, a single bubble is released from the needle submerged in the tank bottom. The bubble rises until it reaches the free surface. It remains at rest for much longer than the surfactant adsorption and desorption times. As mentioned in Section 2, this means that the surfactant molecules adsorb onto the liquid-air interface so that the surface density $\widehat{\Gamma}$ of both the bath and bubble surfaces takes the equilibrium value $\widehat{\Gamma}_{\rm eq}$. Then, the water film between the bubble and the bath surface drains and breaks up, and the bubble bursting begins.

The entire process leading to the formation of the jet droplets takes a time much shorter than the characteristic adsorption and desorption times [16,17,22]. This implies that the surfactant adsorbed onto the interface at the initial instant remains in the monolayer during the bubble bursting. There may be a transfer of molecules from the adsorbed monolayer toward the bulk only during the fast compression of interface elements where the monolayer is saturated. In this sense, the surfactant can be regarded as insoluble even though it is present as a solute in the liquid phase. The surface diffusion time is also much larger than the characteristic time of the process. Therefore, surfactant diffusion over the interface can be ignored.

Suppose we neglect the effect of the gas. In that case, the bubble bursting is essentially characterized by the bubble radius $R = [3V/(4\pi)]^{1/3}$ (V is the bubble volume), the liquid density ρ and viscosity μ, the characteristic surface tension σ_c, and the gravity acceleration g. Two dimensionless numbers can be defined based on these quantities: the Bond number $B = \rho g R^2/\sigma_c$ and the Ohnesorge number $\mathrm{Oh} = \mu/\left(\rho R \sigma_c\right)^{1/2}$.

In the presence of the surfactant, we choose the equilibrium (initial) value $\sigma_{\rm eq} = \sigma(\widehat{\Gamma}_{\rm eq})$ as the characteristic surface tension σ_c. In this way, the initial states for given values of B and Oh are geometrically similar without and with surfactant. In other words, the initial bubble shapes scaled with the bubble radius R are identical with and without surfactant, provided that B and Oh take the same values.

As mentioned above, the surfactant can be considered insoluble in terms of the characteristic time of the process. For a fixed surfactant-liquid system, its effect on the bubble bursting can be characterized only in terms of $\Gamma_{\rm eq} = \widehat{\Gamma}_{\rm eq}/\widehat{\Gamma}_\infty$.

We scale the bubble shape with the bubble radius R and define the dimensionless time $t^* = t/t_c$, where $t_c = (\rho R^3/\sigma_{\rm eq})^{1/2}$ is the inertio-capillary time. The origin of time $t^* = 0$ is the instant when the free surface reversal occurs at the bubble bottom.

Considering the above dimensional analysis, one concludes that

$$\mathcal{S} = \mathcal{S}(B, \mathrm{Oh}, \Gamma_{\rm eq}, t^*), \tag{1}$$

where $\mathcal{S}$ represents the dimensionless bubble shape. In the next section, we study the effect of $\Gamma_{\rm eq}$ on $\mathcal{S}$ by comparing scaled images of the bubble bursting with and without surfactant for the same values of B, Oh, and t^*. This comparison allows one to isolate the effects of *local* soluto-capillarity and Marangoni stress on the bubble dynamics, as explained below.

The dimensionless numbers $\{B, \mathrm{Oh}, t^*\}$ are the only independent quantities that involve the dimensional independent parameters $\{g, R, \rho, \mu, \sigma_{\rm eq}, t\}$. Suppose those numbers take the same values in two experiments with and without surfactant. One can interpret the results assuming that the two experiments are characterized by the same values of $\{g, R, \rho, \mu, \sigma_{\rm eq}, t\}$. Therefore, the differences between the bubble dimensionless shapes with and without surfactant must be attributed only to the capacity of the surfactant monolayer to produce variations of surface tension over the bubble surface, which gives rise to *local* soluto-capillarity and Marangoni stress.

In other words, we can assume that two scaled images obtained for the same values of $\{B, \mathrm{Oh}, t^*\}$ but with and without surfactant correspond to two bubbles with the same values of $\{g, R, \rho, \mu, \sigma_{\rm eq}, t\}$. The images differ because $\sigma_{\rm eq}$ remains constant during the bubble evolution in the surfactant-free case, while this quantity changes over the free surface of a surfactant-covered bubble due to the monolayer dynamics.

As mentioned above, we conducted experiments with glycerin/water mixtures to determine the effects of the surfactant monolayer on the bubble bursting. For this purpose, the Bond and Ohnesorge number of the mixture must match those of the corresponding surfactant-covered bubble case. The density, viscosity, and surface tension of a glycerine/water mixture are known functions of the glycerin concentration. It must be noted that glycerin concentration has a relatively small influence on the density and surface tension for the range of glycerin concentration considered in our analysis. However, the viscosity drastically depends on the concentration. Based on this idea, we followed this iterative procedure. We select a specific glycerin concentration. Using the target Bond number, we obtain the bubble radius. This value and the target Ohnesorge number are used to calculate the viscosity. We compare this result with the viscosity of the selected glycerin concentration. If the difference is larger than 10%, we modify the glycerin concentration accordingly and repeat the process. Once the assumed and obtained viscosity values differ by less than 10%, we select the needle radius to obtain the bubble radius determined in the calculations.

4. Results

The bubble bursting can be split into two stages: (i) the bubble shrinkage and deformation due to the collapse of capillary waves before the free surface reversal ($t^* < 0$), and (ii) the jet formation after the free surface reversal ($t^* > 0$). This last part includes the growth of the capillary waves on the jet surface, which, in most cases, lead to the free surface pinching and the ejection of droplets.

In this section, we analyze the effect of the surfactant monolayer on each of the two stages mentioned above by comparing the dimensionless shapes $\mathcal{S}$ of the bubbles with and without surfactants for approximately the same values of $\{B, \mathrm{Oh}, t^*\}$. We describe in detail the bubble dynamics for two semidilute monolayers ($\Gamma_{\rm eq} < 1$), a quasi-saturated monolayer ($\Gamma_{\rm eq} \simeq 1$ with $c/c_{\rm cmc} \lesssim 0.5$), and a saturated monolayer ($\Gamma_{\rm eq} = 1$ with $c/c_{\rm cmc} \gtrsim 0.5$).

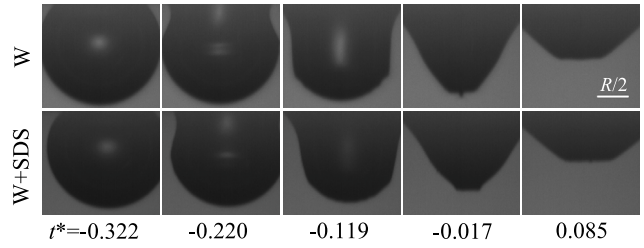

Fig. 3. Images of the cavity collapse for $B = 0.13$ and Oh = 0.0038. The upper and lower images correspond to $\Gamma_{eq} = 0$ and 0.545, respectively. The images have been scaled with the bubble radius R (which took different values with and without surfactant).

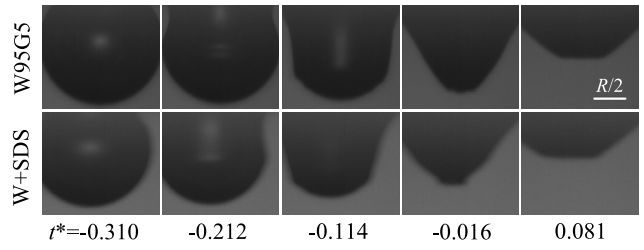

Fig. 4. Images of the cavity collapse for $B = 0.15$ and Oh = 0.0043. The upper and lower images correspond to $\Gamma_{eq} = 0$ and 0.806, respectively. The images have been scaled with the bubble radius R (which took different values with and without surfactant).

4.1. Semidilute monolayers ($\Gamma_{eq} \simeq 0.545$ and 0.806)

The results of this section are analyzed in light of the numerical simulation of Constante-Amores et al. [11] for the base case with $\Gamma_{eq} = 1/4$. It must be noted that this simulation corresponds to a surfactant much more diffusive than SDS. Therefore, the effects associated with the surfactant non-homogeneous distribution are expected to be larger in our experiments.

According to Constante-Amores et al. [11], the converging capillary wave transports surfactant toward the bottom of the bubble, giving rise to a local decrease in surface tension there. Depending on the bubble surface region, the surface tension gradient produces Marangoni stress favoring or opposing the cavity collapse. The net effect of the Marangoni stress is to delay this process. This is observed in Fig. 3, which compares the dimensionless bubble shapes for approximately the same values of B, Oh, and t^* with and without surfactant. Consider, for instance, the time to the interface reversal $t^* = -0.017$. The surfactant-loaded bubble is closer to the interface reversal than its surfactant-free counterpart. However, the dimensionless time to the interface reversal is the same. This means that the surfactant delays the subsequent process that leads to cavity wave collapse. Considering the dimensional analysis in Section 3, we conclude that the bursting of a surfactant-covered bubble takes longer than the bursting of a surfactant-free bubble with the same equilibrium surface tension.

The delay of the cavity collapse can also be attributed to the global soluto-capillarity effect caused by the bubble shrinkage, which reduces the average surface tension and increases the characteristic capillary time. Besides, the surfactant surface density increases at the bubble bottom due to the surfactant convection toward that region and the surface compression there [11]. Therefore, the surface tension is expected to decrease sharply in that region. This local soluto-capillarity effect may also contribute to the cavity collapse delay. It is impossible to separate the effects of the Marangoni stress and soluto-capillarity experimentally.

The toroidal capillary wave triggered at the initial stage of the bubble bursting travels toward the bubble bottom, forming a cusp-like region there. The images right before the free surface reversal in Figs. 3 and 4 ($t^* = -0.017$ and -0.016 for $\Gamma_{eq} = 0.545$ and 0.806, respectively) show that the size of that cusp decreases in the presence of surfactant due to local reduction of the capillary pressure there. This may also suggest that the surfactant monolayer affects the damping of short-wavelength waves caused by viscosity.

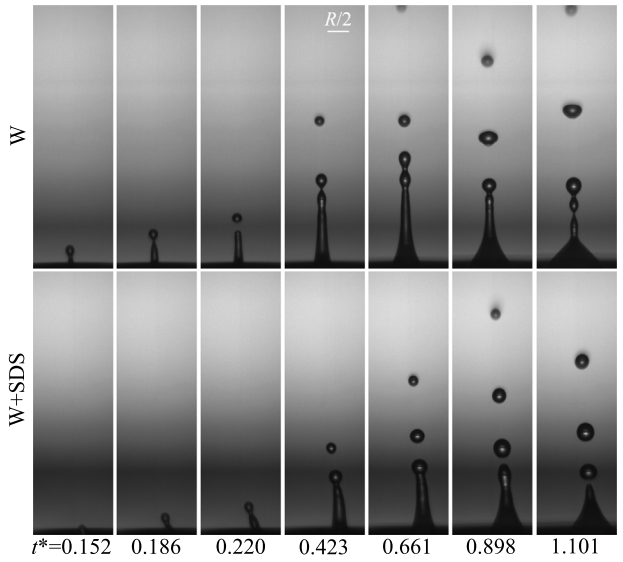

Fig. 5. Images of the jet and droplet formation for $B = 0.13$ and Oh = 0.0038. The upper and lower images correspond to $\Gamma_{eq} = 0$ and 0.545, respectively. The images have been scaled with the bubble radius R (which took different values with and without surfactant).

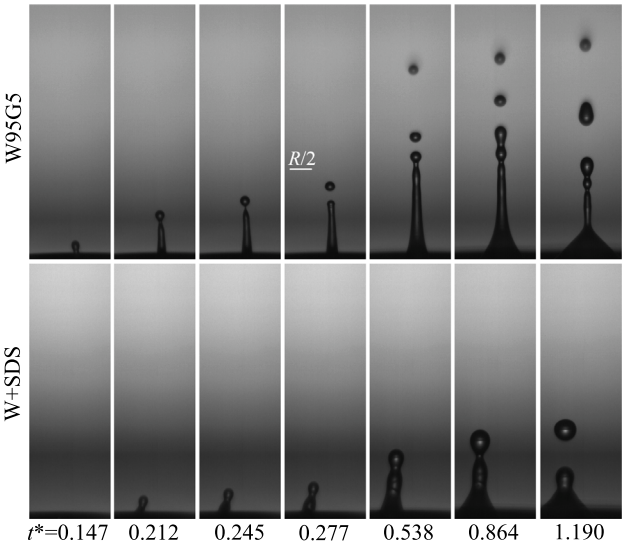

Fig. 6. Images of the jet and droplet formation for $B = 0.15$ and Oh = 0.0043. The upper and lower images correspond to $\Gamma_{eq} = 0$ and 0.806, respectively. The images have been scaled with the bubble radius R (which took different values with and without surfactant).

The simulations of Constante-Amores et al. [11] indicate that Marangoni stresses induce a recirculation zone close to the jet base. This effect opposes the flow from the jet bottom toward the front. The larger pressure gradient in the surfactant-free case leads to longer jets with more pronounced bulbous regions at their tips. Our experiments also show that longer and faster jets are produced without the SDS monolayer (Figs. 5 and 6). However, one cannot conclude that the bulbous regions are more pronounced at their tips.

It is difficult to anticipate whether the surfactant concentration on the surface of the ejected droplets increases or decreases with respect to the initial value Γ_{eq}. On one side, the flow is expected to convect

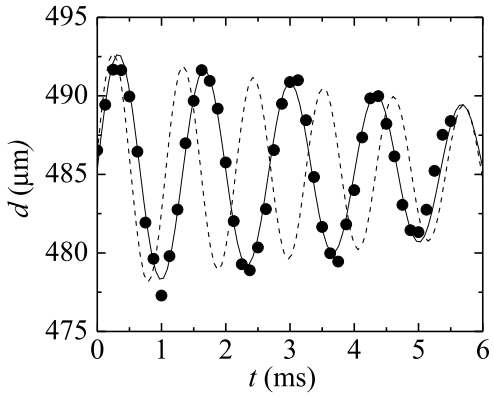

Fig. 7. Droplet vertical size $d(t)$ of the first-ejected droplet for $B = 0.15$, Oh = 0.0043, and $\Gamma_{eq} = 0.806$. The solid line is the fit of the function $d(t) = d_d + ae^{-\gamma t}\cos(\omega_d t + \phi)$ to the experimental data. The dashed line is the same function but with the frequency $\omega_d = 5.8$ rad/ms corresponding to $\Gamma = \Gamma_{eq}$.

the surfactant molecules toward the precursor jet surface. On the other side, a new free surface is created when the jet grows. The amount of surfactant trapped in the jet droplets results from the competition between these two factors. The simulations of Constante-Amores et al. [11] show that the surfactant concentration of the ejected droplets is higher than Γ_{eq}. A similar effect has been observed by Ji et al. [23] when nano/microsized particulates are present in the liquid reservoir.

The frequency of the quadrupole oscillation of a surfactant-covered droplet is essentially affected by the decrease in the surface tension due to the surfactant monolayer. Interfacial elasticity and surface viscosities can significantly affect the oscillation damping rate, but their influence on the frequency is secondary [24]. Therefore, the quadrupole mode frequency is approximately given by the equation $\omega_d = 8(\rho d_d^3/\sigma_d)^{-1/2}$ [25,26], where d_d and σ_d are the droplet diameter and average surface tension, respectively.

The first-ejected droplet oscillates while moving upwards. The small-amplitude oscillations are the superposition of several oscillation modes. The quadrupole oscillation has the smallest damping rate and, therefore, becomes dominant as the oscillation amplitude decreases.

We measured the distance $d(t)$ between the north and south poles of the first-ejected droplet by processing the images with a subpixel resolution technique [27] (Fig. 7). Then, we obtained the diameter d_d and frequency ω_d by fitting the function $d(t) = d_d + ae^{-\gamma t}\cos(\omega_d t + \phi)$ to the experimental data for very small oscillation amplitudes. In this way, we calculated the surface tension σ_d and the corresponding surfactant density given by the isotherm $\Gamma_d(\sigma_d)$.

The above calculations led to ($d_d = 243.3$ μm, $\omega_d = 13.7$ rad/s) and ($d_d = 485.2$ μm, $\omega_d = 4.7$ rad/ms) for $\Gamma_{eq} = 0.545$ and 0.806, respectively. The corresponding surface tensions were $\sigma_d = 42.2$ and 39.3 mN/m, respectively. The surface coverage was $\Gamma_d \simeq 1.0$ in the two cases. As shown in Fig. 7, the oscillation frequency corresponding to Γ_{eq} significantly deviates from that observed in the experiments. We conclude that the convection of surfactant molecules toward the jet tip increases the surface coverage until the monolayer becomes practically saturates. This suggests that the flow enhances the mass transfer of contaminants (surfactants) to the atmosphere by bubble bursting.

4.2. Quasi-saturated monolayer ($\Gamma_{eq} \simeq 1$ with $c/c_{cmc} \lesssim 0.5$)

The bursting of a bubble covered with a quasi-saturated monolayer of SDS constitutes a special case because slight spatial variations of the surface coverage produce large gradients of surface tension (Fig. 2c) and, therefore, intense Marangoni stresses. Fig. 8 shows the strong influence of the surfactant monolayer on the interface dynamics at the free surface reversal. In the presence of the surfactant, the size of the

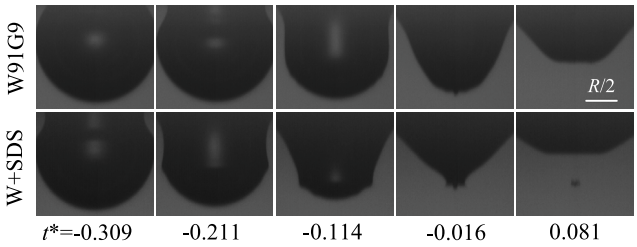

Fig. 8. Images of the cavity collapse for $B = 0.15$ and Oh = 0.0049. The upper and lower images correspond to $\Gamma_{eq} = 0$ and 0.992, respectively. The images have been scaled with the bubble radius R (which took different values with and without surfactant).

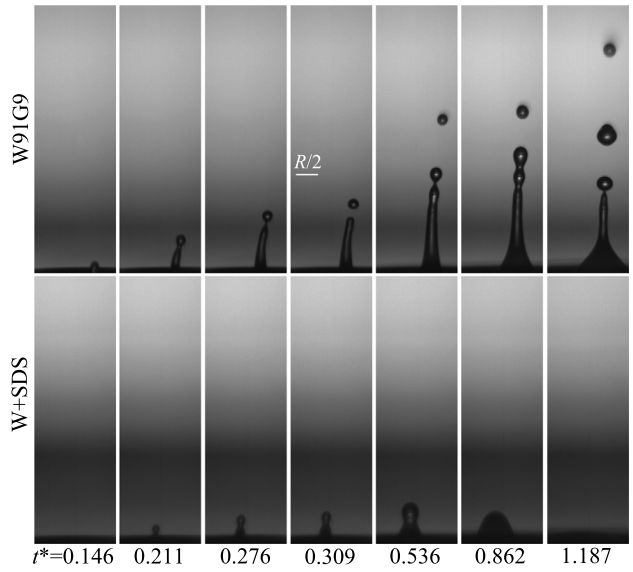

Fig. 9. Images of the jet and droplet ejection for $B = 0.15$ and Oh = 0.0049. The upper and lower images correspond to $\Gamma_{eq} = 0$ and 0.992, respectively. The images have been scaled with the bubble radius R (which took different values with and without surfactant).

cusp formed right before the free surface reversal decreases. The free surface reversal is preceded by the formation of a tiny bubble. This effect was observed in none of our experiments without surfactant, probably because the Ohnesorge number took very low values. The ejection of this tiny bubble suggests that Marangoni convection favors the pinching of the diminutive gas thread created before the surface reversal. We will come back to this point below.

Interestingly, the quasi-saturated surfactant monolayer suppresses the end-pinching mechanism responsible for the ejection of liquid droplets (Fig. 9). This phenomenon has also been observed by Pierre et al. [15].

The surfactant-driven escape from end-pinching in contracting nearly-inviscid and moderately viscous filaments has been nicely described from numerical simulations by Kamat et al. [22] and Constante-Amores et al. [28], respectively. The surfactant accumulates in the stagnation region near the nascent jet neck. This results in a large surface density gradient on the immediate blob-side of the neck. The resulting Marangoni stress drives liquid in the opposite direction to the inertio-capillary flow thinning the neck, which generates a vortex next to the curved free surface. This effect prevents the thinning of the neck. Then, the jet escapes the end-pinching mechanism, and the neck reopens. The intense Marangoni stresses produced by the quasi-saturated SDS monolayer in bubble bursting are responsible for the same mechanism as that described above for contracting filaments.

The formation of a tiny bubble at the bottom of the cavity is consistent with the suppression of the end-pinching mechanism in the

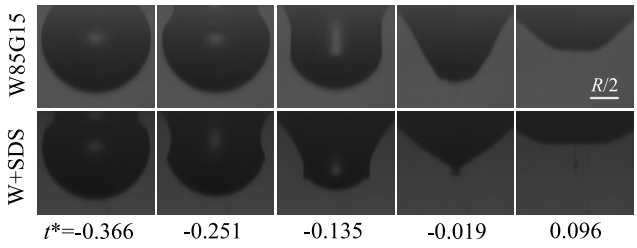

Fig. 10. Images of the cavity collapse for $B = 0.13$ and Oh = 0.0064. The upper and lower images correspond to $\Gamma_{eq} = 0$ and 1, respectively. The images have been scaled with the bubble radius R (which took different values with and without surfactant).

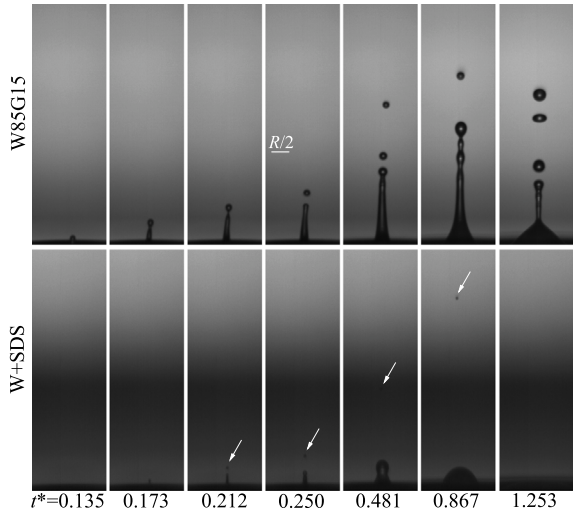

Fig. 11. Images of the jet and droplet ejection for $B = 0.13$ and Oh = 0.0064. The upper and lower images correspond to $\Gamma_{eq} = 0$ and 1, respectively. The images have been scaled with the bubble radius R (which took different values with and without surfactant). The arrows point at the ejected diminutive droplet.

liquid jet. In both cases, the Marangoni stress pumps the liquid toward the neck, where the surfactant surface density decreases [22]. This flow opposes the neck thinning when the liquid is the inner phase, while the opposite occurs in a gas thread surrounded by the liquid.

4.3. Saturated monolayer ($\Gamma_{eq} = 1$ with $c/c_{cmc} \gtrsim 0.6$)

As in the experiments with quasi-saturated monolayers, the size of the cusp formed right before the free surface reversal decreases in the presence of a saturated SDS monolayer (Fig. 10). In addition, the free surface reversal is also preceded by the free surface breakup, leading to the formation of a tiny bubble. The intense Marangoni stress at the jet's surface suppresses the end-pinching mechanism. However, a diminutive droplet escapes in the early stage of the jet formation (see Fig. 11). As shown below, the velocity of this only droplet is similar to that of the first-ejected droplet without surfactant. Sharp variations of the droplet radius are found for $0.6 \lesssim c/c_{cmc} \lesssim 1$. The radius of ejected droplet becomes essentially independent of c for concentrations larger than the critical micellar concentration.

The formation of the tiny droplet described above is completely reproducible. This intriguing phenomenon entails the drastic reduction of the spatial scale characterizing the free surface reversal. This may be explained by the sharp decrease in the capillary pressure due to the surfactant accumulation at the bubble bottom. Marangoni stresses do not suppress the end-pinching mechanism in the precursor jet, probably due to the increase of the Ohnesorge number characterizing that tiny jet.

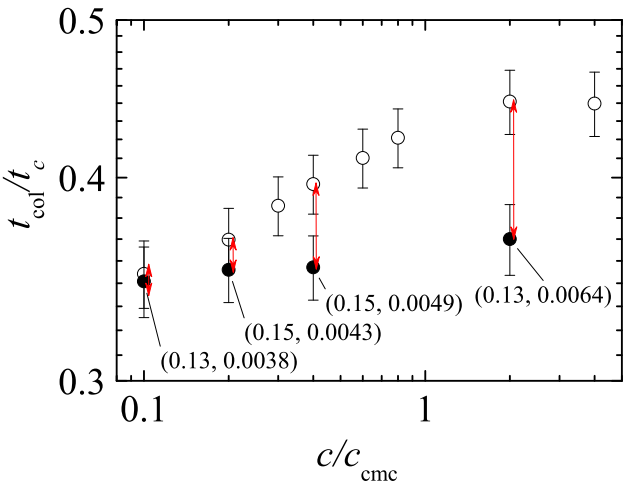

Fig. 12. Cavity collapse time t_{col} as a function of the SDS concentration c for a fixed diameter of the injection needle. The arrows indicate the correspondence between the collapse time with surfactant and that for the glycerine/water mixture with the same Bond and Ohnesorge numbers. The labels indicate the approximate values (B,Oh) of those numbers. The error bars indicate the experimental uncertainty.

4.4. Delay of the cavity collapse

We have measured the cavity collapse time for all the surfactant concentrations. The results have been compared with those for glycerine/water mixtures characterized by the same values of the Bond and Ohnesorge numbers (Fig. 12). This comparison allows us to determine quantitatively the effect of local soluto-capillarity and Marangoni stress on the cavity collapse time. It must be pointed out that the effect of the global reduction of the water–air surface tension due to the presence of a surfactant monolayer has been eliminated from the analysis by calculating the collapse time in terms of the inertio-capillary time $t_c = (\rho R^3/\sigma_{eq})^{1/2}$ based on the equilibrium surface tension σ_{eq} instead of that of the clean interface.

As can be observed, local soluto-capillarity and/or Marangoni stress delay the bubble collapse. This delay increases with the surfactant concentration and reaches a practically constant value for saturated monolayers.

4.5. Radius and velocity of the first-ejected droplet

We now analyze the dependency of the radius R_d and velocity v_d of the first-ejected droplet on the SDS concentration c for a fixed diameter of the injection needle. The experiments correspond to the parameter region indicated in Fig. 13. The surface tension and, therefore, the radius of the bubble released by the needle decreases as c increases. This implies that the Ohnesorge (Bond) number increases (decreases) as c increases. There is an experimental realization in which no droplet was ejected. This occurs even though the small parameter region explored in our experiments is far from that where no droplet is ejected without surfactant.

We compare our experimental results with the theoretical prediction derived by Gañán-Calvo and López-Herrera [8] to separate the surfactant effect from that of B and Oh. Fig. 14 allows one to obtain the following conclusions:

- For $c/c_{cmc} \lesssim 0.4$ ($\Gamma_{eq} \lesssim 0.99$), there is a sharp decrease in the droplet velocity while the radius remains practically constant.
- For $0.4 \lesssim c/c_{cmc} \lesssim 0.5$ ($\Gamma_{eq} \simeq 1$), the jet does not emit any droplets. As explained above, this can be explained in terms of the strong Marangoni stress caused by the sharp dependence of σ on Γ for these concentrations (Fig. 2). The Marangoni stress suppresses the end-pinching mechanism.

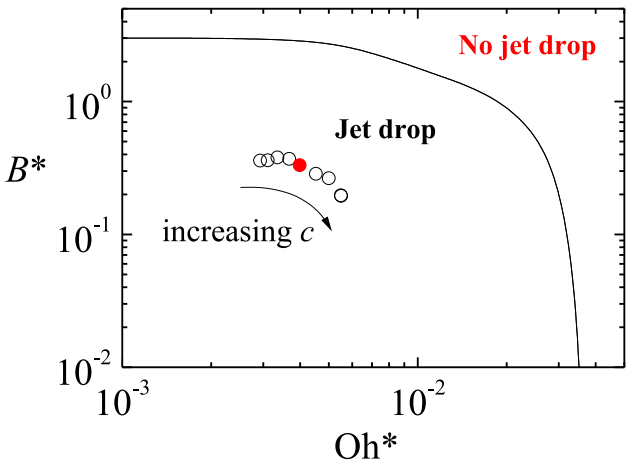

Fig. 13. Parameter region where jet drops are produced without surfactant [10]. The open (solid) symbols correspond to experimental realizations where droplets were (were not) produced. The Bond and Ohnesorge numbers, B^* and Oh*, are defined in terms of the cap radius.

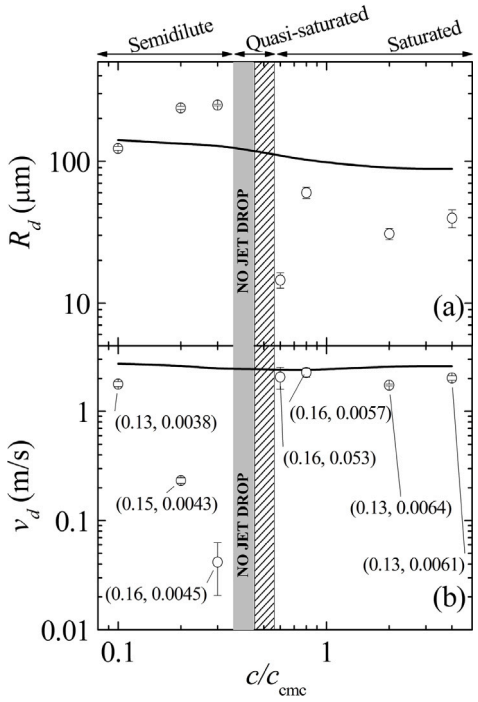

Fig. 14. Radius R_d and velocity v_d of the first-ejected droplet as a function of the SDS concentration c for a fixed diameter of the injection needle. The gray areas correspond to the values of surfactant concentration for which no droplet was ejected in any experimental realization. The striped areas correspond to the values of surfactant concentration for which a droplet was ejected in some experimental realizations. The labels indicate the approximate values (B,Oh) of the Bond and Ohnesorge numbers. The error bars indicate the experimental uncertainty.

- A tiny only droplet ($R_d \simeq 10$ μm) is ejected at $c/c_{\text{cmc}} \simeq 0.6$. The velocity of that droplet is approximately independent of c. The radius becomes approximately constant for $c \gtrsim c_{\text{cmc}}$.

The comparison with the theoretical prediction of Gañán-Calvo and López-Herrera [8] indicates that none of the effects described above can be attributed to the variation of the Ohnesorge and Bond numbers.

5. Conclusions

We have analyzed the bursting of a bubble covered with an insoluble surfactant. The experiments have been compared with those of surfactant-free bubbles characterized by the same Bond and Ohnesorge numbers values to determine the surfactant monolayer's effect.

The bursting of a surfactant-covered bubble takes longer than the bursting of a surfactant-free bubble with the same equilibrium surface tension, probably due to the interfacial elasticity. The surfactant monolayer produces quantitative effects on the cavity collapse, altering the shape and size of the cusp formed at the bottom right before the free surface reversal. The surfactant is dragged by the flow toward the jet tip so that the monolayer covering the first-emitted droplet practically saturates.

Quasi-saturated monolayers qualitatively change the bubble bursting due to the sharp dependence of the surface tension on the SDS surface density for $\hat{\Gamma}_{\text{eq}} \simeq \hat{\Gamma}_{\infty}$. A tiny bubble is formed at the cavity bottom for values of B and Oh for which this phenomenon does not occur without surfactant. In addition, the jet escapes from the end-pinching mechanism. As a consequence, there is a small interval of $\hat{\Gamma}_{\text{eq}}$ for which no jet droplet is emitted. Both tiny bubble ejection and the surfactant-driven escape from end-pinching are caused by the liquid flow driven by the intense Marangoni stress.

For a sufficiently large surfactant concentration, a diminutive droplet manages to escape from the jet before the end-pinching mechanism is suppressed. The droplet is much smaller than its surfactant-free counterpart but moves at a similar speed.

We would like to emphasize that the local reduction of the surface tension due to inhomogeneous surfactant distribution (local solutocapillarity effect) and the Marangoni stress resulting from the surfactant concentration gradient are intrinsically linked. It is practically impossible to separate one from another experimentally. To determine their separate effects, one needs to solve a theoretical model and "turn off" one of them in the equations, as done by Constante-Amores et al. [11].

The present work can be extended along several lines. One of them is to study the effect of a surfactant monolayer for Ohnesorge numbers close to the critical value Oh=0.034 [8], for which energy focusing at the cavity bottom is optimum.

We do not expect the ionic character of the surfactant to affect the phenomenon because the latter occurs in the absence of electric fields. Of course, other surfactants exhibiting different dependencies of the surface tension up on the surfactant surface density can affect differently the bubble bursting. However, this work aims not to conduct such an exhaustive analysis but to show the importance of a surfactant monolayer in this phenomenon.

CRediT authorship contribution statement

E.J. Vega: Methodology, Investigation, Validation, Formal analysis, Visualization, Writing – review & editing. **J.M. Montanero:** Conceptualization, Methodology, Formal analysis, Visualization, Writing – original draft, Writing – review & editing.

Declaration of competing interest

The authors declare that they have no known competing financial interests or personal relationships that could have appeared to influence the work reported in this paper.

Data availability

Data will be made available on request.

Acknowledgments

Support from the Spanish Ministry of Science and Innovation (grants no. PID2019-108278RB-C32 / AEI/10.13039/501100011033 and PID2022-140951OB-C22) and Gobierno de Extremadura (grant no. GR21091) is gratefully acknowledged.

References

[1] L. Deike, Mass transfer at the ocean–atmosphere interface: The role of wave breaking, droplets, and bubbles, Annu. Rev. Fluid Mech. 54 (2022) 191–224.
[2] F. MacIntyre, Flow patterns in breaking bubbles, J. Geophys. Res. 77 (1972) 5211–5228.
[3] J.M. Boulton-Stone, J.R. Blake, Gas bubbles bursting at a free surface, J. Fluid Mech. 254 (1993) 437–466.
[4] L. Duchemin, S. Popinet, C. Josserand, S. Zaleski, Jet formation in bubbles bursting at a free surface, Phys. Fluids 14 (2002) 3000–3008.
[5] H. Lhuissier, E. Villermaux, Bursting bubble aerosols, J. Fluid Mech. 696 (2012) 5–44.
[6] A.M. Gañán-Calvo, Revision of bubble bursting: Universal scaling laws of top jet drop size and speed, Phys. Rev. Lett. 119 (2017) 204502.
[7] J.M. Gordillo, J. Rodriguez-Rodriguez, Capillary waves control the ejection of bubble bursting jets, J. Fluid Mech. 867 (2019) 556–571.
[8] A.M. Gañán-Calvo, J.M. López-Herrera, On the physics of transient ejection from bubble bursting, J. Fluid Mech. 929 (2021) A12.
[9] E. Ghabache, A. Antkowiak, C. Josserand, T. Seon, On the physics of fizziness: How bubble bursting controls droplets ejection, Phys. Fluids 26 (2014) 121701.
[10] P.L.L. Walls, L. Henaux, J.C. Bird, Jet drops from bursting bubbles: How gravity and viscosity couple to inhibit droplet production, Phys. Rev. E 92 (2015) 021002(R).
[11] C.R. Constante-Amores, L. Kahouadji, A. Batchvarov, S. Shin, J. Chergui, D. Juric, O. Matar, Dynamics of a surfactant-laden bubble bursting through an interface, J. Fluid Mech. 911 (2021) A57.
[12] J. Feng, M. Roché, D. Vigolo, L.N. Arnaudov, S.D. Stoyanov, T.D. Gurkov, G.G. Tsutsumanova, H.A. Stone, Nanoemulsions obtained via bubble-bursting at a compound interface, Nat. Phys. 10 (2014) 606–612.
[13] Z. Yang, B. Ji, J.T. Ault, J. Feng, Enhanced singular jet formation in oil-coated bubble bursting, Nat. Phys. 19 (2023) 884–890.
[14] J.M. Boulton-Stone, The effect of surfactant on bursting gas bubbles, J. Fluid Mech. 302 (1995) 231–257.
[15] J. Pierre, M. Poujol, T. Seon, Influence of surfactant concentration on drop production by bubble bursting, Phys. Rev. Fluids 7 (2022) 073602.
[16] M. Roche, M. Aytouna, D. Bonn, H. Kellay, Effect of surface tension variations on the pinch-off behavior of small fluid drops in the presence of surfactants, Phys. Rev. Lett. 103 (2009) 264501.
[17] H.C. Mayer, R. Krechetnikov, Landau-Levich flow visualization: Revealing the flow topology responsible for the film thickening phenomena, Phys. Fluids 24 (2012) 052103.
[18] A. Ponce-Torres, M. Rubio, M.A. Herrada, J. Eggers, J.M. Montanero, Influence of the surface viscous stress on the pinch-off of free surfaces loaded with nearly-inviscid surfactants, Sci. Rep. 10 (2020) 16065.
[19] K. Tajima, M. Muramatsu, T. Sasaki, Radiotracer studies on adsorption of surface active substance at aqueous surface. I. Accurate measurement of adsorption of Tritiated Sodium Dodecylsulfate, Bull. Chem. Soc. Jpn. 43 (1970) 1991–1998.
[20] K. Takamura, H. Fischer, N.R. Morrow, Physical properties of aqueous glycerol solutions, J. Pet. Sci. Eng. 98–99 (2012) 50–60.
[21] C. Ferrera, J.M. Montanero, M.G. Cabezas, An analysis of the sensitivity of pendant drops and liquid bridges to measure the interfacial tension, Meas. Sci. Technol. 18 (2007) 3713–3723.
[22] P.M. Kamat, B.W. Wagoner, A.A. Castrejón-Pita, J.R. Castrejón-Pita, C.R. Anthony, O.A. Basaran, Surfactant-driven escape from endpinching during contraction of nearly inviscid filaments, J. Fluid Mech. 899 (2020) A28.
[23] B. Ji, A. Singh, J. Feng, Water-to-air transfer of nano/microsized particulates: Enrichment effect in bubble bursting jet drops, Nano Lett. 22 (2022) 5626–5634.
[24] H.-L. Lu, R.E. Apfel, Shape oscillations of drops in the presence of surfactants, J. Fluid Mech. 222 (1991) 351–368.
[25] J.W.S.R. Lord, On the capillary phenomena of jets, Proc. R. Soc. Lond. Ser. A Math. Phys. Eng. Sci. 29 (1879) 71–97.
[26] A. Ponce-Torres, J.M. Montanero, M.A. Herrada, E.J. Vega, J.M. Vega, Influence of the surface viscosity on the breakup of a surfactant-laden drop, Phys. Rev. Lett. 118 (2017) 024501.
[27] E.J. Vega, J.M. Montanero, J. Fernández, On the precision of optical imaging to study free surface dynamics at high frame rates, Exp. Fluids 47 (2009) 251–261.
[28] C.R. Constante-Amores, L. Kahouadji, A. Batchvarov, S. Shin, J. Chergui, D. Juric, O.K. Matar, Dynamics of retracting surfactant-laden ligaments at intermediate Oh number, Phys. Rev. Fluids 5 (2020) 084007.